



Design and simulation of novel laparoscopic renal denervation system: a feasibility study

Eunbi Ye, Jinhwan Baik, Seunghyun Lee, Seon Young Ryu, Sunchoel Yang, Eue-Keun Choi, Won Hoon Song, Hyeong Dong Yuk, Chang Wook Jeong & Sung-Min Park

To cite this article: Eunbi Ye, Jinhwan Baik, Seunghyun Lee, Seon Young Ryu, Sunchoel Yang, Eue-Keun Choi, Won Hoon Song, Hyeong Dong Yuk, Chang Wook Jeong & Sung-Min Park (2018) Design and simulation of novel laparoscopic renal denervation system: a feasibility study, International Journal of Hyperthermia, 35:1, 9-18, DOI: [10.1080/02656736.2018.1468037](https://doi.org/10.1080/02656736.2018.1468037)

To link to this article: <https://doi.org/10.1080/02656736.2018.1468037>



© 2018 The Author(s). Published with license by Taylor & Francis Group, LLC



Published online: 18 May 2018.





Submit your article to this journal [↗](#)



View Crossmark data [↗](#)

Design and simulation of novel laparoscopic renal denervation system: a feasibility study

Eunbi Ye^a , Jinhwan Baik^a, Seunghyun Lee^a, Seon Young Ryu^a, Sunchoel Yang^b, Eue-Keun Choi^c, Won Hoon Song^d, Hyeong Dong Yuk^d, Chang Wook Jeong^d and Sung-Min Park^a 

^aDepartment of Creative IT Engineering, POSTECH, Pohang, Republic of Korea; ^bDepartment of Prototype Production, Osong Medical Innovation Foundation, Chungbuk, Republic of Korea; ^cDepartment of Internal Medicine, Seoul National University Hospital, Seoul, Republic of Korea; ^dDepartment of Urology, Seoul National University Hospital, Seoul, Republic of Korea

ABSTRACT

Purpose: In this study, we propose a novel laparoscopy-based renal denervation (RDN) system for treating patients with resistant hypertension. In this feasibility study, we investigated whether our proposed surgical instrument can ablate renal nerves from outside of the renal artery safely and effectively and can overcome the depth-related limitations of the previous catheter-based system with less damage to the arterial walls.

Method: We designed a looped bipolar electrosurgical instrument to be used with laparoscopy-based RDN system. The tip of instrument wraps around the renal artery and delivers the radio-frequency (RF) energy. We evaluated the thermal distribution via simulation study on a numerical model designed using histological data and validated the results by the *in vitro* study. Finally, to show the effectiveness of this system, we compared the performance of our system with that of catheter-based RDN system through simulations.

Results: Simulation results were within the 95% confidence intervals of the *in vitro* experimental results. The validated results demonstrated that the proposed laparoscopy-based RDN system produces an effective thermal distribution for the removal of renal sympathetic nerves without damaging the arterial wall and addresses the depth limitation of catheter-based RDN system.

Conclusions: We developed a novel laparoscope-based electrosurgical RDN method for hypertension treatment. The feasibility of our system was confirmed through a simulation study as well as *in vitro* experiments. Our proposed method could be an effective treatment for resistant hypertension as well as central nervous system diseases.

ARTICLE HISTORY

Received 11 December 2017
Revised 27 March 2018
Accepted 17 April 2018

KEYWORDS

Biological modelling; hypertension; numerical simulation; radiofrequency ablation; renal denervation

Introduction

Hypertension is a growing global public health problem due to multiple reasons, including an aging population and the rising rates of obesity [1,2]. Approximately 10% of patients diagnosed with hypertension have resistant hypertension, which is defined as blood pressure that remains above the desired level despite treatment with three antihypertensive agents of different classes [1] and blood pressure that is controlled using more than four medications [2]. Resistant hypertension is a serious condition leading to various life-threatening clinical complications, such as heart failure, stroke, renal failure and heart disease [1,3]. Thus, treating resistant hypertension clinically is very important for the patient's longevity and quality of life.

Sympathetic nerves play an important role in long-term blood pressure regulation in humans [4,5]. The increased sympathetic activity has been implicated as the primary precursor of hypertension in both humans and in animal models [6]. Furthermore, there is growing evidence that abnormal renal function in hypertension is due to the increased activity

of renal sympathetic nerves [7]. Thus, an open surgical procedure to remove renal sympathetic nerves for treating hypertension called Sympathectomy was employed in 1930 [8–10]. Although this technique provided effective treatment, its use was discontinued because of its highly invasive nature and associated complications, such as perioperative morbidity, mortality and long-term complications [11,12].

Recently, a minimally invasive procedure called renal denervation (RDN) system has been developed as an effective method to remove renal nerves for treating resistant hypertension. The RDN procedure selectively removes the hyperactive renal sympathetic nerves using a radiofrequency (RF) ablation technique, thus controlling hypertension. A catheter-based RDN system, a prominent representative system for the RDN procedure, has demonstrated promising results with minimal side effects in nonrandomized studies and unblinded randomised trials [13–15]. However, a recent phase-III randomized controlled trial, investigating the efficacy and safety of this procedure, have found that the catheter-based RDN is not effective and shows no improvement

CONTACT Sung-Min Park  sungminpark@postech.ac.kr  drboss@gmail.com

© 2018 The Author(s). Published with license by Taylor & Francis Group, LLC

This is an Open Access article distributed under the terms of the Creative Commons Attribution License (<http://creativecommons.org/licenses/by/4.0/>), which permits unrestricted use, distribution, and reproduction in any medium, provided the original work is properly cited.

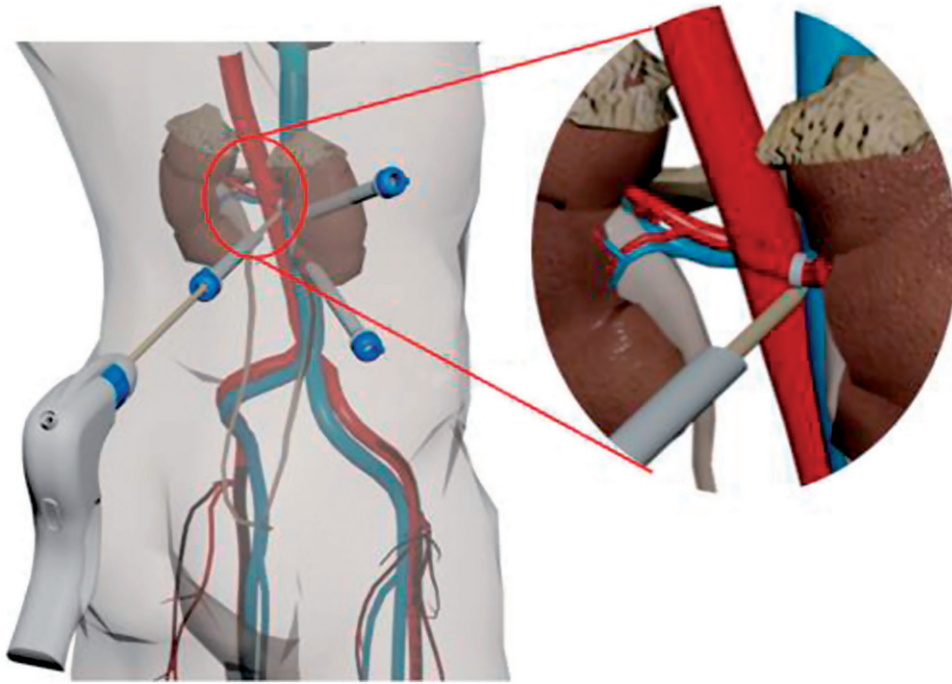


Figure 1. Schematic drawing of proposed laparoscopy-based RDN surgical approach.

in outcomes of patients with resistant hypertension when compared with the outcomes of the sham procedure [16]. The primary limitation of the catheter-based RDN system, found through histopathological evaluation of the renal artery, is that the electrodes placed inside the lumen of the artery cannot deliver RF energy effectively to all the renal nerve bundles along the renal artery, especially to the nerves present beyond 2 mm from the lumen surface [17]. Since sympathetic nerves are located at a distance of 0.5–10 mm from the intima layer of the artery with approximately 31% of the nerves located between 2 and 10 mm from the lumen–intima interface [18,19], the catheter-based system could not deliver sufficient energy to treat the hyperactive nerves. Higher RF energy could be used to destroy these distant nerves but may severely damage the intima layer resulting in serious side effects, such as stenosis. The secondary limitation of the catheter-based approach is that it could not directly monitor the temperature rise near the renal nerves outside the artery during or after the treatment.

In the absence of effective surgical treatment for resistant hypertension, a laparoscopic approach has been proposed as an alternative method to overcome the limitations of the catheter approach [20]. According to Gerber et al. [20], the laparoscopic approach is capable of removing nerves that are typically not removed by RF-based catheter ablation. The claim by Gerber et al. is promising, there have been no studies published to describe the surgical strategy or instrument design for the effective laparoscopy-based RDN system. In this study, for the first time, we propose a laparoscopy-based RDN system design that ablates the renal nerves from the exterior of the renal artery by wrapping it around. We demonstrate its feasibility of this system using the numerical model developed based on clinical data and validated through extensive *in vitro* experiments. This system demonstrates the feasibility of the effective denervation of the renal

nerve present between 0.5 and 10 mm from the arterial lumen. We confirmed the superiority of our system over the catheter-based RDN system via simulations based on performance. Our results demonstrate that a practical laparoscopic system could be developed for the surgical treatment of resistant hypertension.

Methods

Proposed surgical system of laparoscopy-based RDN

Our surgical RF ablation plan is shown in Figure 1. The tissues surrounding the renal artery is excised from the dorsal side through trocars to expose the renal artery to allow easy access for the surgical instruments to perform RF ablation. The retroperitoneal approach using three trocars is minimally invasive and reduces the likelihood of complications because there is no peritoneal violation is involved.

Our surgical tip design objectives were threefold: (1) to completely remove renal sympathetic nerves without damaging the renal artery, (2) to minimize the damage to the surrounding tissues by focusing RF heating within the contour of the wrapped electrode, and (3) to be flexible enough to adapt to different renal artery sizes. Figure 2 shows the conceptual design of the proposed surgical instrument with a looped electrode that meets the desired design objectives. To localize the heating proximal to the electrodes, the tip structure was configured to be bipolar, wherein both electrodes were placed side by side. The RF current, which flows between the electrodes, rapidly attenuates as the distance of the tissue from the electrodes increases. To completely remove renal nerves distributed around the artery, the electrode, which is the end part of the surgical instrument, was designed to wrap around the renal artery such that RF energy is delivered to completely remove sympathetic nerves distributed around the artery. As shown in

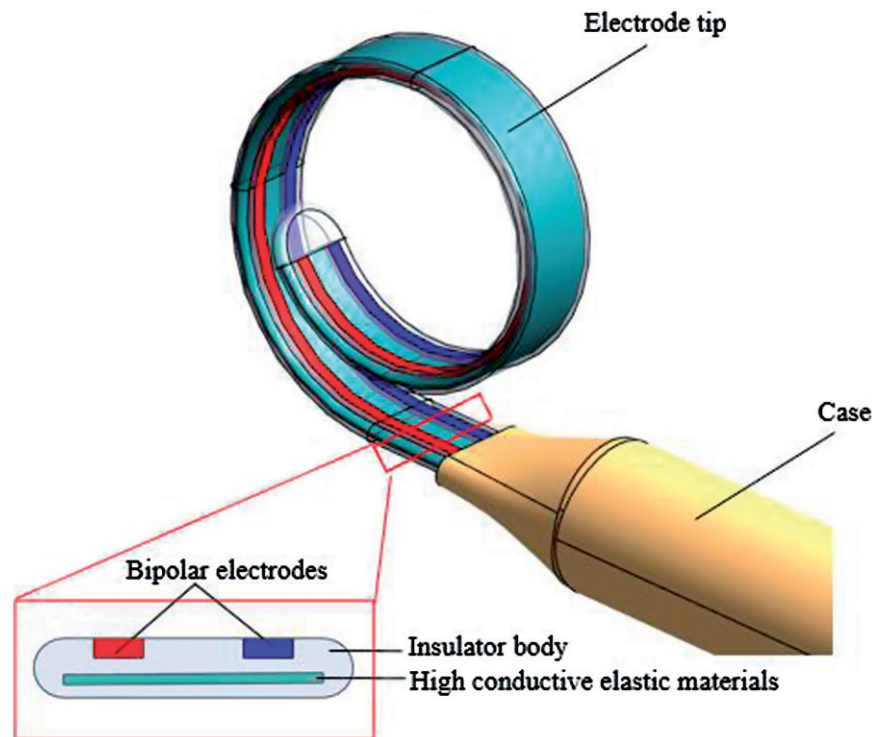


Figure 2. Concept design of the surgical instrument for laparoscopy-based RDN.

Figure 2, a strip of highly conductive elastic material was placed under the electrodes. Due to its elasticity, the tip remains flat within the case of the surgical instrument while entering the body and starts to wrap around the artery when the tip is pushed out of the case at the surgical site. This elastic strip also allows the tip to fit to different sizes of the renal artery. In addition, the strip is made of highly conductive material to reduce the RF field radiating to the posterior part of the electrode due to the electromagnetic shielding effect of electrically high conductive materials [21]. Therefore, with the metal strip, RF energy in the rear side of the electrode is minimized preventing any damage to the normal tissues at the site.

Computational modelling

Tissue modelling

In our previous study, we analyzed the anatomical distribution of sympathetic nerve fibers around the renal artery using the nephrectomy tissues from humans. We showed that approximately 31% of the renal sympathetic nerves are located beyond 2 mm from the arterial lumen [19]. To reflect our previous findings in tissue modelling, we developed a realistic three-dimensional (3D) numerical model based on the thinnest of the 174 tissue slides obtained at 40 μm intervals, from a representative tissue. Then, we developed a simplified simulation model shown in Figure 3(b). In this model, the renal artery diameter was 5 mm, the lumen diameter was 2 mm, and the thickness of the blood vessel wall was 1.5 mm. The four renal sympathetic nerves were modelled at 2 mm, 2.5 mm, 3 mm, and 3.5 mm because 90% of the nerve fibers are located within 4 mm from the luminal surface of the renal artery, based on our histological studies. In addition, to verify the RF field radiating to the outside of the surgical tip, a renal vein located posterior to the renal

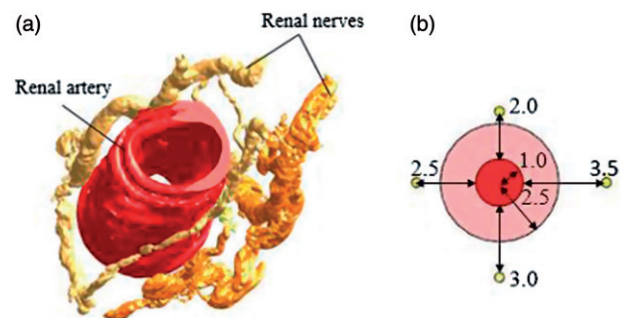


Figure 3. (a) A realistic computable 3D model generated by histological analysis. (b) Simplified 3D phantom [mm]. The model includes the renal nerves and renal arterial wall.

artery was modelled with an outer wall diameter of 10 mm, lumen diameter of 8.6 mm, and wall thickness of 0.7 mm [22].

The surrounding tissue environment was modelled in two cases depending on the surgical approach. For the laparoscopy-based RDN system shown in Figure 4(a), the tissues between the artery and electrodes were assigned as fat and nerves and the surrounding environment outside the surgical instrument was assigned gaseous CO_2 , which is commonly used in laparoscopic surgeries; because the perinephric fat and Gerota's fascia enclosing the kidney need to be incised via a laparoscopic surgical approach. For the catheter-based RDN system shown in Figure 4(b), the surrounding tissue was modelled as fat to represent the catheter-based procedure. Table 1 lists the properties of the materials included in the simulation.

RF ablation tip modelling

The proposed RF ablation tip was simulated for RF energy and resulting heat distribution using the Sim4life

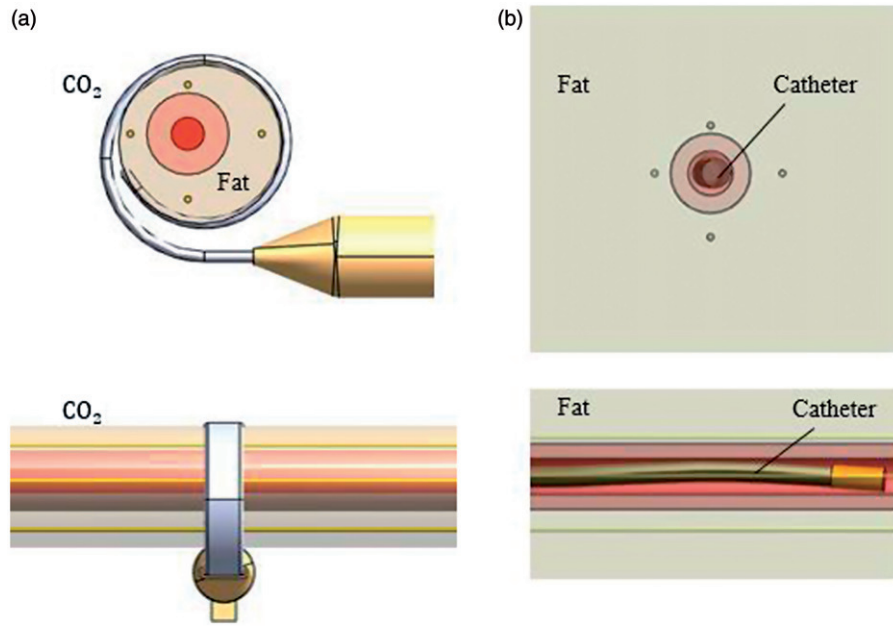


Figure 4. Finite element modelling: (a) laparoscopy-based RDN, (b) catheter-based RDN.

Table 1. Electrical and thermal properties of the materials.

	ρ [kg/m ³] ^a	σ [S/m] ^b	κ [W/m/K] ^c	HR [W/m ³ /K] ^d
Blood	1049	0.659	0.517	709,090
Blood vessel wall	1101	0.232	0.462	11160.7
Nerve	1075	0.265	0.490	11642.5
Fat	911	0.057	0.212	2012.8
CO ₂	1.977	0	0.017	0
Gel				
Setting 1	950	0.23	0.605	0
Setting 2		0.65		

^a ρ = material density, ^b σ = electric conductivity, ^c κ = thermal conductivity, ^dHR = heat-transfer rate.

computational electromagnetic analysis software. The gap between the bipolar electrodes was 2 mm, the width of the highly conductive metal strip was 3 mm, and the total width of the tip was 5 mm such that the surgical device can be inserted through the 5 mm trocar that is commonly used in a laparoscopic procedure. While performing simulations, all conductive materials were assigned as stainless steel and insulation materials were assigned as polyimide.

To compare the safety and efficacy between the catheter- and laparoscopy-based systems, a simplified 6F catheter-based Symplicity Flex (Medtronic, Santa Rosa, CA, USA) with an outer diameter of 2 mm and an inner diameter of 1.8 mm was modelled [23].

Numerical simulation setup

Computational calculation of the temperature distribution around the electrodes and tissues during RF injection was performed using Sim4life V3.4 software (ZMT, Zurich, Switzerland). Sim4life is a simulation platform that provides computational human phantoms with multi-physics solvers and advanced tissue models. The multiphysics solvers include the full electromagnetic wave, quasi-static electromagnetic and thermodynamic solvers. This tool is useful for developing novel devices, optimizing design parameters, increasing the

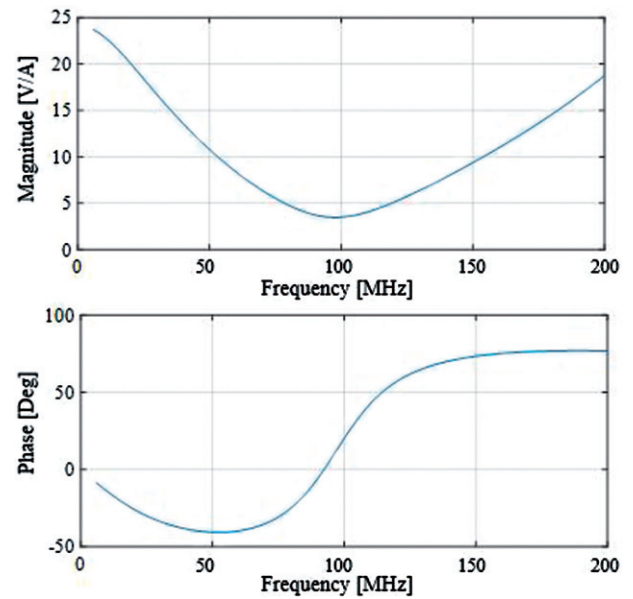


Figure 5. Input impedance of the prototype electrode as a function of frequency.

knowledge regarding energy delivery and determining induced heating [24].

Computation of electric fields

The frequency of the source RF current was 1 MHz, which is considerably less than the resonant frequency of 100 MHz, as shown in Figure 5. Quasi-static electromagnetic solver was used to calculate low-frequency electromagnetic problems [25] with the following equation:

$$\nabla \cdot \tilde{\epsilon} \nabla \varnothing = 0 \quad (1)$$

where $\tilde{\epsilon}$ is the complex electric permittivity and \varnothing is a scalar potential. The electromagnetic field was recorded to use as a heat source for the thermal simulations.

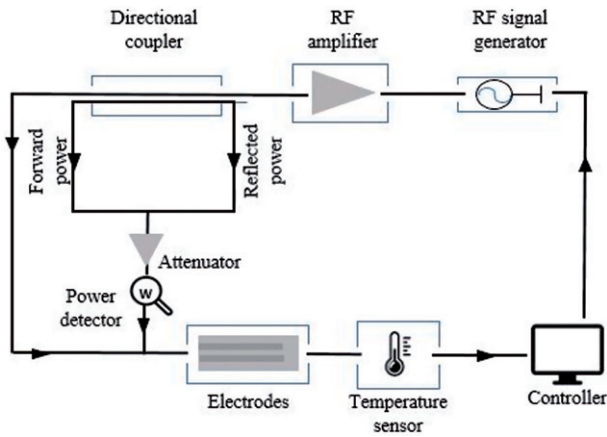


Figure 6. Experimental system for simulation validation.

Temperature distribution computation

The temperature changes in the tissues during RF ablation were calculated using the following Pennes bioheat Equation (2), which has been extensively used to solve computational bio-electromagnetic problems since its introduction [26].

$$\rho c \frac{\partial T}{\partial t} = \nabla \cdot (k \nabla T) + \rho Q + \rho S - \rho_b \rho \omega (T - T_b) \quad (2)$$

where ρ is the material density, c is the specific heat capacity, T is the tissue temperature, k is the thermal conductivity, Q is the metabolic heat generation rate, S is the specific absorption rate, and ω is the perfusion rate. The term ' $\rho_b c_b \rho \omega$ ' is sometimes referred as the heat-transfer rate (HR). The perfusion rate of blood was set at 10,000 ml/min/kg [27] to examine the blood cooling effect according to the blood perfusion rate.

Experimental validation setup

To validate the numerical simulation technique of the RF ablation device, *in vitro* experiments were conducted, and the results were extensively compared with the results of the simulations performed under the same conditions. For the *in vitro* experiments, we constructed a prototype tip and evaluated the heating effects of the tip at nine measurement points. The experimental system for delivering RF energy to the device and measuring the temperature profile during RF injection is shown in Figure 6. The system comprised an RF generator (Tektronix, AFG3101), RF amplifier (Minicircuit, LZY-22+), power sensor (Keysight, U2004A), and directional coupler (Minicircuit, ZABDC50-150HP+). The system was controlled by the LabVIEW 2013 software. The prototype tip comprised three layers: a metal strip, insulation and two electrodes placed 2 mm apart to support bipolar mode. Stainless steel 304 (SUS304) was used for the construction of the electrodes and metal strip for RF blocking, and the plate was insulated using a polyimide film. The tip was 24 mm \times 110 mm, and the electrodes were 2 mm \times 100 mm (Figure 7(a)).

The experiment was conducted with 6 L gel mixed with polyacrylic acid and NaCl in a 160 mm \times 430 mm \times 170 mm acrylic water tank. The gel had two conductivity settings as

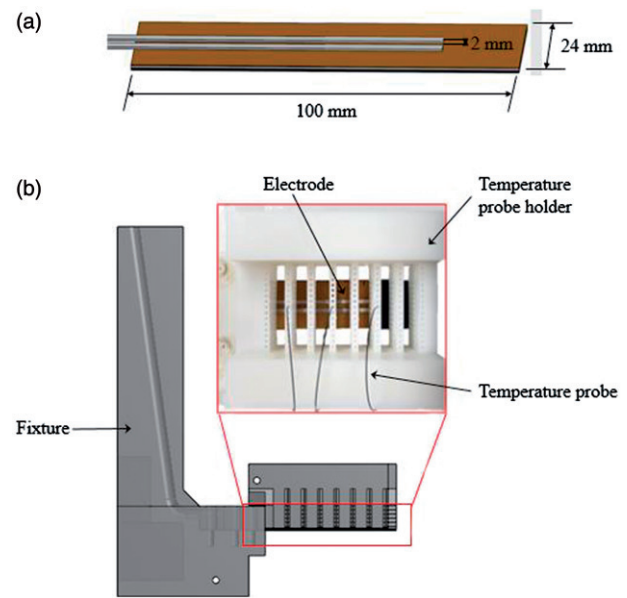


Figure 7. (a) Schematic representation of a prototype tip. (b) Temperature measurement setup. The tip is fixed by the fixture and is connected to coaxial cable. The temperature is inserted into through the holder and measures the temperature on the tip. The temperature is measured at nine points, three points for each three axes.

shown in Table 1: 0.23 S/m (setting 1) and 0.65 S/m (setting 2). The conductivities of the gels reflected those of the blood vessel walls and blood, respectively, because they are affected thermally during RDN. Dielectric properties of gels were measured by a network analyzer (Keysight, E5061B). The input power was switched on for 6 min [28] and then off for 1 min at 1 MHz. The source was connected to the electrode via a coaxial cable.

Temperature distribution near the prototype tip was measured using a fiber optic thermometry system (Luxtron, m600), which can minimize the potential electromagnetic interference (Figure 7(b)). Temperature probes were fixed at the openings in the temperature probe holder that was fabricated using a 3D printer (3D Systems, Project MJP 2500). The spacing between openings was 10 mm along the x-axis and 2.5 mm along both y- and z-axes to facilitate the measurement at different locations. The fixture holding temperature probe kept the temperature sensors in position relative to the electrodes for simultaneous temperature measurement. The experimental protocol is shown in Figure 8. The measurements were repeated six times for each gel setting in the three axial directions, thus resulting in 36 measurements. The electromagnetic simulations were performed with the same initial parameters as in the experiments. The temperature data of both the simulation and validation experiments were normalised by the difference between the initial and average temperatures during the last 60 s of the power-on period.

Results

In this section, we validated the numerical model via *in vitro* studies by comparing the simulated heating results of the simplified surgical device tip with the measured results

under the same condition *in vitro*. We then use this validated model to conduct extensive simulation studies for our proposed laparoscopy-based RDN tip design with the simplified anatomical phantom that was constructed based on histological analysis.

Simulation method validation

The simulated temperature distribution around the prototype tip is shown in Figure 9. The temporal temperature data in the simulation results were extracted at the same points measured in the *in vitro* experiment. The similarity of thermal patterns during RF ablation between the extracted temperature in the simulations and the measured temperature in the *in vitro* studies for settings 1 and 2 are shown in Figure 10. The error bars denote ± 2 standard deviations for each 60 s time interval, indicating a 95% confidence interval for the repeated experimental temperature measurements. In Table 2, time constants (τ), average standard deviation (SD) and error values (E), calculated as the maximum differences

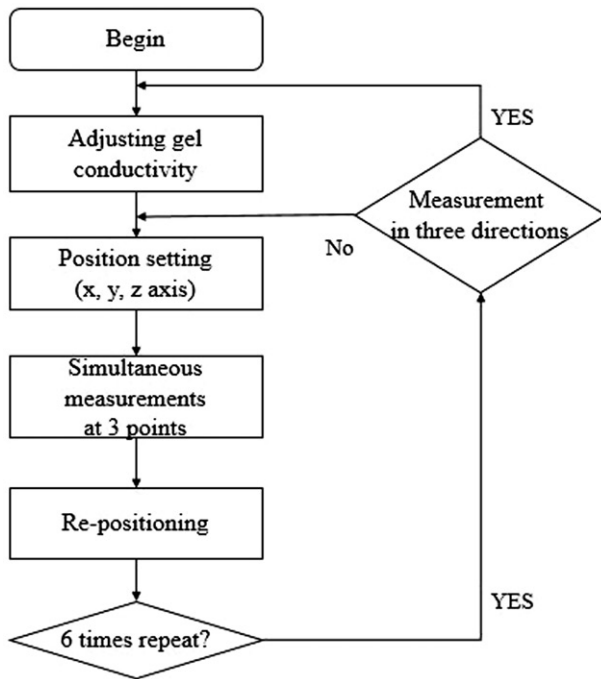


Figure 8. Experimental validation protocol. Experiments were conducted with the same protocol for setting 1 and setting 2, respectively.

between the experimental and simulation results, and maximum error (Max E) are presented for both the settings. The simulation results were within 95% confidence intervals of the experimental results during the RF injection. The average standard deviation was 0.0312, and the average error was 2.7%, indicating that the simulation results reflected the actual temperatures observed during experiments.

These validation results confirmed the excellent agreement between the simulation and experimental results except for a few discrepancies. These discrepancies arose between simulation and *in vitro* experiments due to the differences in placement of the temperature probe between simulation and *in vitro* experiments. The simulation results were based on the temperatures at the center of each opening. However, the temperature probe location could not be fixed in the *in vitro* because the diameter of the temperature probe holder (1.2 mm) was larger than that of the temperature probe diameter (0.6 mm). Figure 11 shows the best heat matching results when the simulation results were obtained with the probe moving across the probe holder along the y-axis. With setting 1, the average error decreased from 2.9% to 1.9%, and with setting 2, the error decreased from 3.7% to 2.8%. These results confirm that the source of discrepancies between the simulations and the *in vitro* experiments mainly arose due to the differences in the placement of the probe and not due to any other fundamental reasons, thus confirming the credibility of the simulation results.

Heat effect on biological tissues

In vitro experiment results confirmed the validity of our numerical simulation technique and we used this numerical technique to simulate the proposed device design in a simplified *in vivo* setting. We performed the thermal simulation on an anatomical phantom for 120 s to obtain the heating pattern distribution within the phantom using our design. The temperature distributions are shown in Figures 12 and 13. Figure 12 shows the normalized thermal distribution in tissues with the laparoscopy-based and catheter-based surgical instruments, where the edge of the red block is the luminal surface and the edge of the blue block is the outer surface of arterial wall. With the laparoscopy-based RDN device, the temperature decreased to approximately 50% of the peak temperature at the outer wall and to 30% of the peak at the luminal surface (Figure 12(c)). With the catheter-

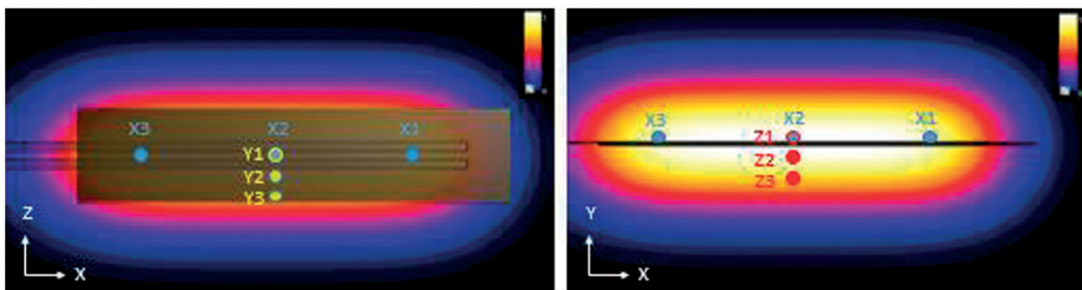


Figure 9. The temperature distribution in the prototype tip model. The model includes the surgical tip and gel. It was normalized with min-max scaling. The temporal temperature profiles were extracted at the same position where the temperature was measured in the experiment marked with white dots (X1, X2, X3, Y1, Y2, Y3, Z1, Z2, Z3).

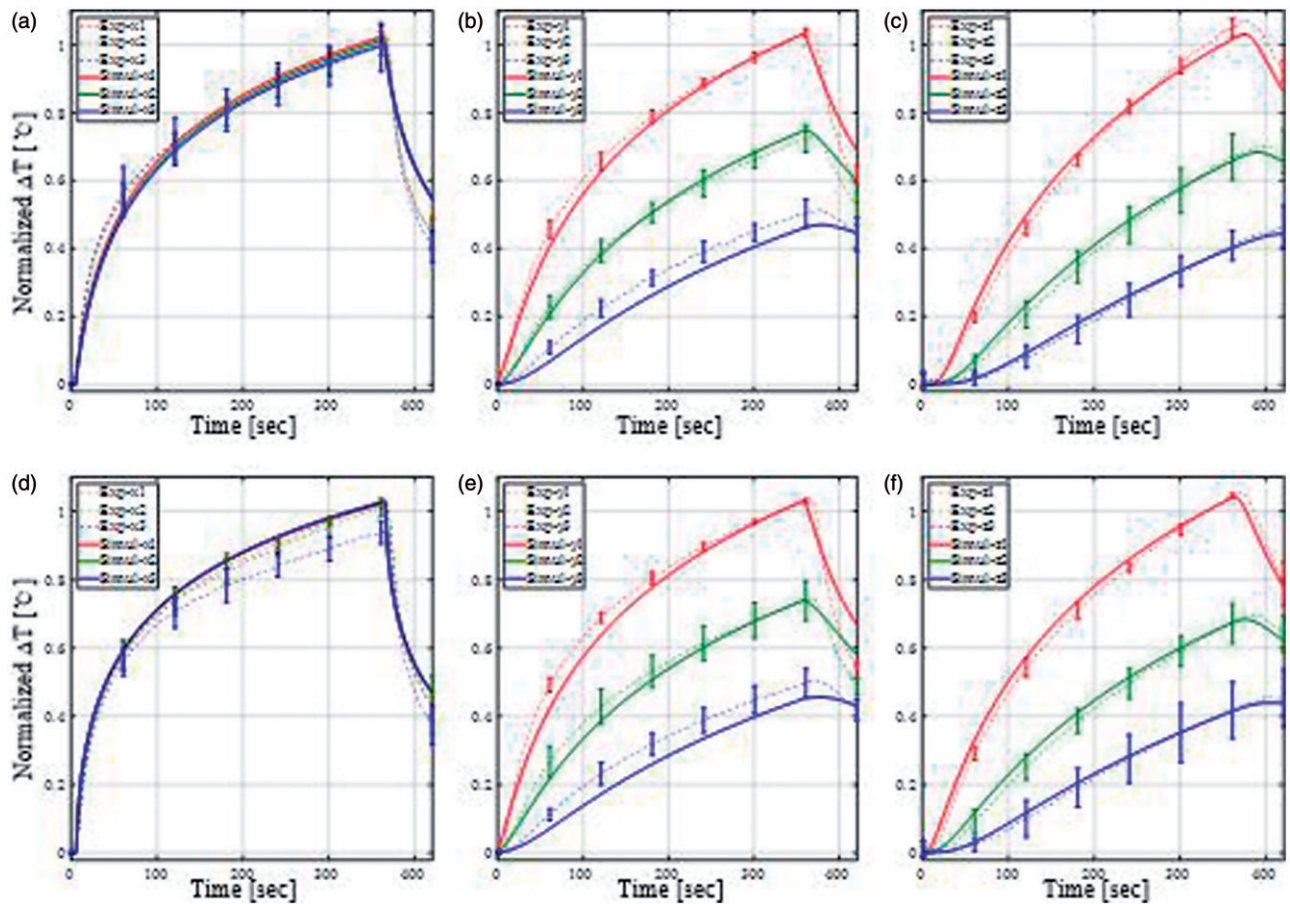


Figure 10. The temporal temperature at the nine measurement positions: (a–c) setting 1 ($\sigma = 0.23$ S/m, $\epsilon = 43$), (d–f) setting 2 ($\sigma = 0.35$ S/m, $\epsilon = 72$). The solid lines represent the simulation results, while the dot lines represent the experiment results. Each graph was normalized by the difference between the initial and average temperatures during the last 60 s of the power-on period.

Table 2. Comparison of experimental and 3-D simulation normalized temperature profiles.

Setting	Axis	Method	τ [sec]	SD	E [%]	Max E [%]
1 $\sigma = 0.23$ S/m, $\epsilon = 43$	x	Exp.	83	0.0320	2.8	13.9
		Simul.	81			
	y	Exp.	110	0.0285	2.9	9.9
		Simul.	116			
	z	Exp.	171	0.0329	1.7	6.4
		Simul.	137			
2 $\sigma = 0.65$ S/m, $\epsilon = 72$	x	Exp.	76	0.0348	3.3	10.3
		Simul.	69			
	y	Exp.	99	0.0222	3.7	13.1
		Simul.	112			
	z	Exp.	150	0.0368	1.7	5.0
		Simul.	132			

based RDN device, the temperatures at outer surface and luminal surface of arterial wall were up to 95% and 85% of the peak temperature, respectively, despite the cooling effect of the blood flow as shown in Figure 12(d). When the temperature of the cell increases above 45°C–50°C, protein breakdown occurs, resulting in cell necrosis [29]. Based on the simulation results obtained with the assumption that the peak temperature generated at the electrode was 60°C, we found that for the laparoscopy-based device the temperature increased to 48°C–58°C at the sympathetic nerves, to 41.6°C at the outer wall of the artery and to 39.3°C at the inner

wall of the artery. For the catheter-based device, under similar conditions, the temperature increased to 46°C–54°C at the renal sympathetic nerve, to 58.9°C at the outer wall of the artery, and to 56.6°C at the inner wall of the artery. We found that the both laparoscopic and catheter-based RDN may result in necrosis at the nerve since the temperature rise for both cases are more than 45°C. However, the results suggests that the laparoscopy-based system is safer since the temperature at the inner wall is lower than 45°C, while the catheter-based system could cause serious damage to inner walls, which results in serious side effects such as stenosis, since the temperature rise is more than 45°C.

Thus, our simulation results clearly show that the laparoscopy-based approach would be safer while effectively eliminating the renal sympathetic nerves. Figure 13 shows the temperature distribution as a function of blood perfusion rate for perfusion rates of 10,000, 5000, and 0 ml/min/kg. As shown in the graph, the temperature inside the artery decreased as the blood perfusion rate increased, resulting in the blood cooling effect. Thus, the lumen inside the artery receives drastically reduced heat from the bipolar electrode located outside the artery.

In the real laparoscopic surgery, the fat surrounding the renal artery are removed, the artery is exposed to allow the wrapping of the renal artery by the surgical tip, and renal vein locates very close to the artery. We modelled the renal

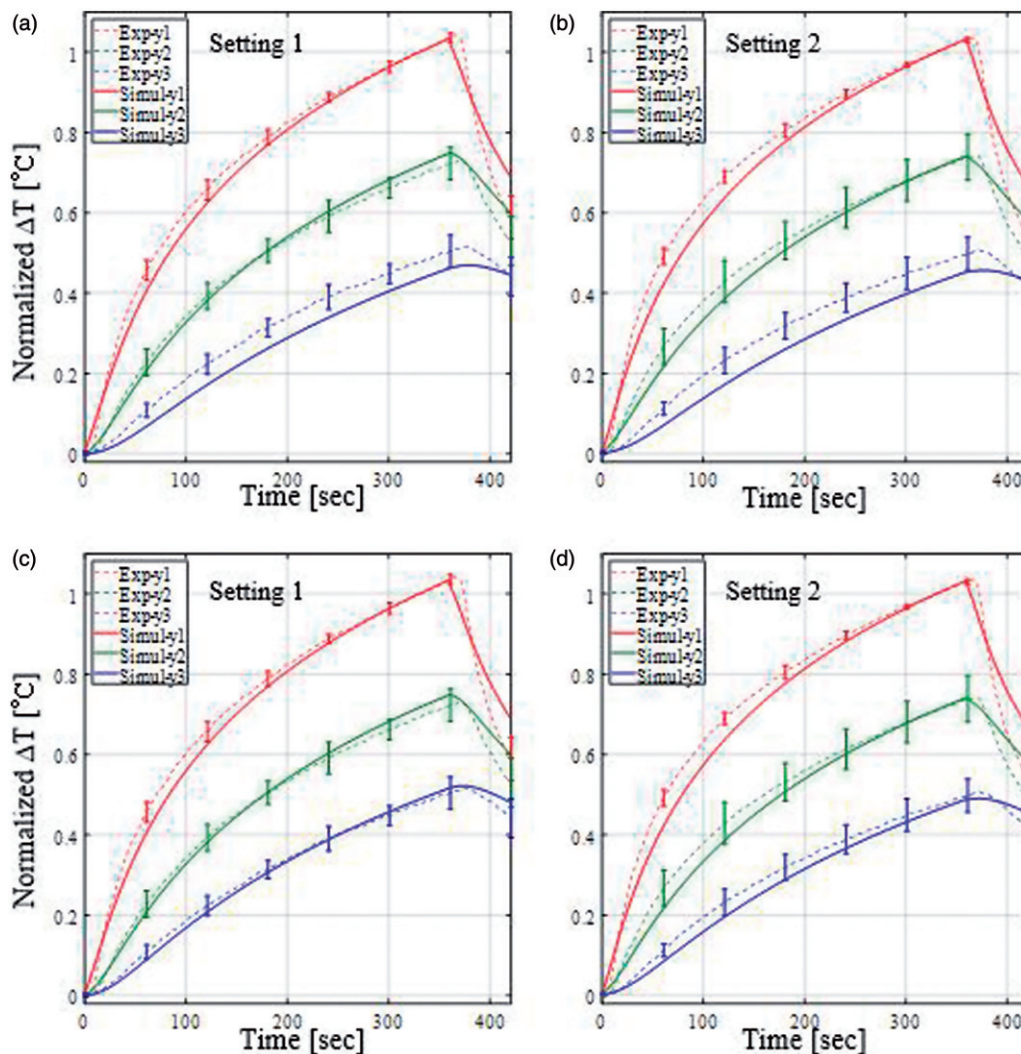


Figure 11. (a–b) Heat pattern matching (Y-component) when all the simulation results were obtained at the center of the temperature probe hole. (c–d) Heat pattern matching (Y-component) when the simulation results obtained with best position optimization in the hole. Each graph was normalized by the difference between the initial and average temperatures during the last 60 s of the power-on period.

vein, which is located posterior to the surgical tip, to examine the effects of heat radiation to the surrounding anatomy. Figure 14 plots the temperature at the renal vein with and without the insertion of metal strip that is posterior to the instrument. The normalized graph demonstrates that the temperature at the vein was slightly elevated without the metal strip while using our device, and thus, safety can be enhanced by reducing the heat radiated to the rear side of the instrument.

Discussion

In this study, we showed proof of concept of a newly designed laparoscopy-based RDN system through simulation study and validation experiments. The high level of agreement between measured and simulated thermal results confirm our findings. Simulation results confirmed that the laparoscopy-based system can address the limitations of the catheter-based system in treating hypertension. The results of numerical simulations showed that heat distributions induced by the electric fields are always greater in regions closer to the electrodes. In addition, blood

perfusion inside the arteries causes a cooling effect resulting in significantly reduced harmful effects compared to the catheter-based approach. Thus, the laparoscopy-based RDN approach, which includes placing the electrodes directly on the nerve outside the artery, can remove the renal nerves more safely and effectively than the catheter-based RDN approach, which includes positioning the electrodes inside the artery. The laparoscopic RDN system has other advantages due to access from the outside of the artery. First, by wrapping the renal arteries completely by a surgical tip, the renal nerves can be completely removed regardless of the distance. Second, by inserting the thermometer into the surgical instruments, the temperature rise in the nerves positioned outside the arteries can be monitored during the procedure allowing stable control and ensuring safety and efficacy.

The main limitation of our study, however, is that we established the feasibility of our design mainly via simulation and *in vitro* studies. In the real-world environment, the behavior of the system could be very different from these simulation results. Thus, as a next step of verification that is closer to the real-world environment, we plan to conduct our

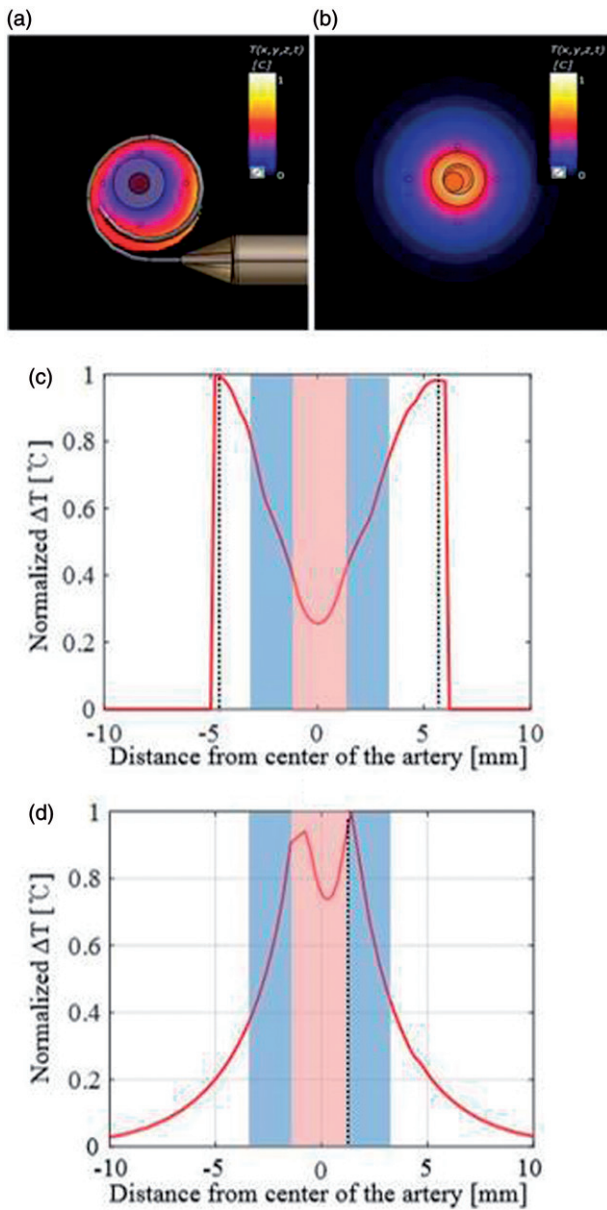


Figure 12. Cross-sectional views of the heat distribution: (a) laparoscopy-based RDN, (b) catheter-based RDN. Two-dimensional temperature profiles: (c) laparoscopy-based RDN, (d) catheter-based RDN (red block: renal arterial lumen, blue blocks: renal arterial wall, black line: position of the electrode). Each graph was normalized with min-max scaling, respectively.

study on an animal surgical model as well as *ex vivo* model along with histological examination to confirm RDN effectiveness and safety of surrounding tissue.

This laparoscopy-based method can change the paradigm of hypertension treatment, and it can also be extended for treating many other diseases caused by abnormalities of the central nervous system, such as sleep apnea, depression and heart diseases. In addition, secondary complications could be prevented through improved primary treatment [1,2,30–33]. When our laparoscopic surgical instrument is developed, it could be applied to the robotic surgical system to establish less invasive and more accurate RDN method. Thus, the development of this novel laparoscopy-based RDN procedure can be significantly beneficial for a wide variety of patient populations.

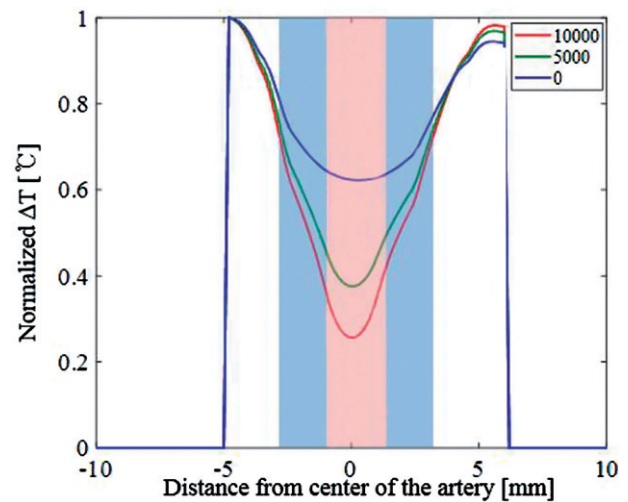


Figure 13. Two-dimensional temperature profiles according to the blood perfusion rate (red block: renal arterial lumen, blue blocks: arterial wall). The graph was normalized with min-max scaling.

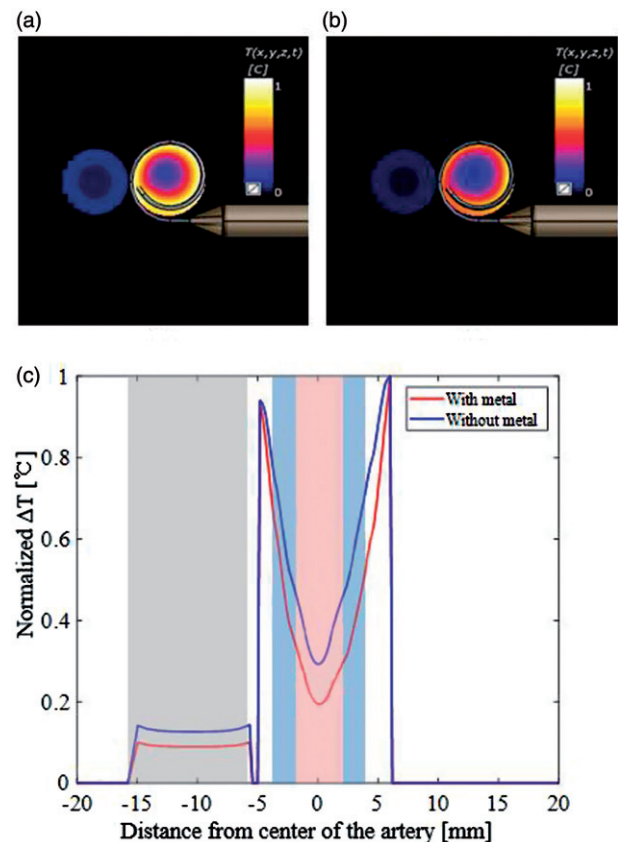


Figure 14. Blocking thermal radiation to the renal vein using Nitinol (conductor): (a) without metal strip and (b) with metal strip. (c) Two-dimensional temperature profiles with or without metal strip (red block: renal arterial lumen, blue block: renal arterial wall, gray block: renal vein). Each data were normalized with minmax scaling, respectively.

Conclusions

In this study, we proposed a novel laparoscopy-based electro-surgical RDN device for resistant hypertension treatment. The thermal distributions induced by this new surgical instrument was evaluated and compared with catheter-based RDN system using simulation method. The simulation results

showed that our device is safer and more effective than the existing catheter-based systems. Our approach, is effective in blocking the sympathetic nerves located even beyond 2 mm from the luminal surface, which are otherwise left untreated by previous catheter-based RDN system. Our *in vitro* experimental results validated the simulation results. Going forward, we will conduct our study on an animal surgical model along with histological examination to confirm RDN effectiveness and safety of surrounding tissue. The success of this system will ultimately provide a safe and effective treatment for resistant hypertension and may also contribute toward the treatment of refractory heart disease, and arterial fibrillation.

Disclosure statement


No potential conflict of interest was reported by the authors.

Funding

This research was supported by the Ministry of Science and ICT (MSIT), Korea, under the ICT Consilience Creative Program [IITP-2018-2011-1-00783] supervised by the Institute for Information & Communications Technology Promotion (IITP), the Korea Health Technology R&D Project through the Korea Health Industry Development Institute (KHIDI) funded by the Ministry of Health & Welfare, Republic of Korea [grant number: HI17C1314], and under the Basic Science Research Program through the National Research Foundation of Korea (NRF) funded by the Ministry of Science and ICT [NRF-2017R1A5A1015596].

ORCID

Eunbi Ye  <http://orcid.org/0000-0002-5927-989X>

Sung-Min Park  <http://orcid.org/0000-0002-8359-8110>

References

- Calhoun DA, et al. Resistant hypertension: diagnosis, evaluation, and treatment. *Circulation*. 2008;117:e510–e526.
- Nwankwo T, et al. Hypertension among adults in the United States: National Health and Nutrition Examination Survey, 2011–2012. *NCHS Data Brief*. 2013;133:1–8.
- World Health Organization. Global health risks: mortality and burden of disease attributable to selected major risks. World Health Organization; 2009.
- Smith PA, et al. Relationship between central sympathetic activity and stages of human hypertension. *Am J Hypertension*. 2004;17:217–222.
- Dibona GF. Sympathetic nervous system and the kidney in hypertension. *Curr Opin Nephrol Hypertension*. 2002;11:197–200.
- Wyss JM. The role of the sympathetic nervous system in hypertension. *Curr Opin Nephrol Hypertension*. 1993;2:265–273.
- Rodrigues AFDAC, de Lima ILB, Bergamaschi CT, et al. Increased renal sympathetic nerve activity leads to hypertension and renal dysfunction in offspring from diabetic mothers. *Am J Physiol Renal Physiol*. 2013;304:F189–F197.
- Newcombe CP, Shucksmith HS, Suffern WS. Sympathectomy for hypertension. *BMJ*. 1959;1:142.
- Allen EV. Sympathectomy for essential hypertension. *Circulation*. 1952;6:131–140.
- Smithwick RH. Surgical treatment of hypertension. *Am J Med*. 1948;4:744–759.
- Morrissey DM, Brookes V, Cooke WT. Sympathectomy in the treatment of hypertension; review of 122 cases. *Lancet*. 1953;1:403–408.
- Schlaich MP, Sobotka PA, Krum H, et al. Renal denervation as a therapeutic approach for hypertension. *Hypertension*. 2009;54:1195–1201.
- Krum H, Schlaich M, Whitbourn R, et al. Catheter-based renal sympathetic denervation for resistant hypertension: a multicentre safety and proof-of-principle cohort study. *Lancet*. 2009;373:1275–1281.
- Dibona GF, Esler M. Translational medicine: the antihypertensive effect of renal denervation. *Am J Physiol Regul Integr Comp Physiol*. 2010;298:R245–R253.
- Schlaich MP, Sobotka PA, Krum H, et al. Renal sympathetic-nerve ablation for uncontrolled hypertension. *N Engl J Med*. 2009;361:932–934.
- Bhatt DL, Kandzari DE, O'Neill WW, et al. A controlled trial of renal denervation for resistant hypertension. *N Engl J Med*. 2014;370:1393–1401.
- Vink EE, Goldschmeding R, Vink A, et al. Limited destruction of renal nerves after catheter-based renal denervation: results of a human case study. *Nephrol Dial Transplant*. 2014;29:1608–1610.
- Atherton DS, Deep NL, Mendelsohn FO. Micro-anatomy of the renal sympathetic nervous system: a human postmortem histologic study. *Clin Anat*. 2012;25:628–633.
- WH, Song, et al. Analysis of anatomical distribution of renal sympathetic nerve fibers and 3D phantom modeling: Study using nephrectomy specimens. Paper presented at: 2017 Annual Meeting of The Korean Urological Association; 2017 Sep 27–29; Seoul, Korea.
- Gerber RC, Bahler CD, Kraus MA, et al. Laparoscopic renal denervation for uncontrolled hypertension due to medication intolerance: a case report. *Am J Kidney Dis*. 2016;68:131–133.
- Chung DDL. Electromagnetic interference shielding effectiveness of carbon materials. *Carbon*. 2001;39:279–285.
- Bonsib SM. Renal veins and venous extension in clear cell renal cell carcinoma. *Mod Pathol*. 2007;20:44–53.
- Kanai T, Krum H. New treatment for old disease: management of resistant hypertension by percutaneous renal sympathetic denervation. *Revista Española de Cardiología (English Ed.)*. 2013;66:734–740.
- Neufeld E, Kyriakou A, Sharma D, et al. Modeling, effect prediction, and planning for EM-and FUS-based thermal treatment. The 8th European Conference on Antennas and Propagation (EuCAP); 2014 April 6–11; Hague: Netherlands. 2014;1483–1487.
- Plonsey R, Heppner DB. Considerations of quasi-stationarity in electrophysiological systems. *Bull Mathemat Biophysics*. 1967;29:657–664.
- Pennes HH. Analysis of tissue and arterial blood temperatures in the resting human forearm. *J Appl Physiol*. 1948;85:5–34.
- Collins CM, Liu W, Wang J, et al. Temperature and SAR calculations for a human head within volume and surface coils at 64 and 300 MHz. *J Magn Reson Imaging*. 2004;19:650–656.
- IEEE Standard for Safety Levels with Respect to Human Exposure to Radio Frequency Electromagnetic Fields, 3 kHz to 300 GHz. IEEE C95.1-2005. Piscataway, NJ: IEEE Standards Association, 2005
- Lounsbury W, Goldschmidt V, Linke CA, et al. The early histologic changes following electrocoagulation. *J Urol*. 1961;86:321–329.
- Malpas SC. Sympathetic nervous system overactivity and its role in the development of cardiovascular disease. *Physiol Rev*. 2010;90:513–557.
- Esler M, Kaye D. Sympathetic nervous system activation in essential hypertension, cardiac failure and psychosomatic heart disease. *J Cardiovasc Pharmacol*. 2000;35:S1–S7.
- Witkowski A, Prejbisz A, Florczak E, et al. Effects of renal sympathetic denervation on blood pressure, sleep apnea course, and glycemic control in patients with resistant hypertension and sleep apnea. *Hypertension*. 2011;58:559–565.
- Böhm M, Linz D, Ukena C, et al. Renal denervation for the treatment of cardiovascular high risk-hypertension or beyond? *Circul Res*. 2014;115:400–409.